








RESEARCH ARTICLE | MARCH 11 2021

Direct visualization of local deformations in suspended few-layer graphene membranes by coupled *in situ* atomic force and scanning electron microscopy

Stefan Hummel ; Kenan Elibol ; Dengsong Zhang ; Krishna Sampathkumar; Otakar Frank ; Dominik Eder; Christian Schwalb; Jani Kotakoski ; Jannik C. Meyer ; Bernhard C. Bayer 



Appl. Phys. Lett. 118, 103104 (2021)

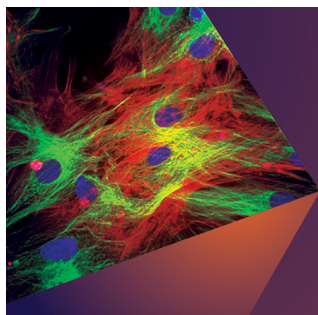
<https://doi.org/10.1063/5.0040522>



Articles You May Be Interested In

A versatile atomic force microscope integrated with a scanning electron microscope

Rev. Sci. Instrum. (May 2017)



Applied Physics Letters

Special Topics Open for Submissions

[Learn More](#)

Direct visualization of local deformations in suspended few-layer graphene membranes by coupled *in situ* atomic force and scanning electron microscopy

Cite as: Appl. Phys. Lett. **118**, 103104 (2021); doi: [10.1063/5.0040522](https://doi.org/10.1063/5.0040522)

Submitted: 14 December 2020 · Accepted: 19 February 2021 ·

Published Online: 11 March 2021



View Online



Export Citation



CrossMark

Stefan Hummel,^{1,2,a)} Kenan Elibol,¹ Dengsong Zhang,³ Krishna Sampathkumar,^{4,5} Otakar Frank,⁴ Dominik Eder,⁶ Christian Schwalb,² Jani Kotakoski,¹ Jannik C. Meyer,^{1,7} and Bernhard C. Bayer^{1,6,a)}

AFFILIATIONS

¹Faculty of Physics, University of Vienna, Boltzmanngasse 5, A-1090 Vienna, Austria

²GETec Microscopy GmbH, Seestadtstrasse 27, A-1220 Vienna, Austria

³Research Center of Nano Science and Technology, International Joint Laboratory of Catalytic Chemistry, Department of Chemistry, College of Sciences, State Key Laboratory of Advanced Special Steel, School of Materials Science and Engineering, Shanghai University, Shanghai 200444, China

⁴J. Heyrovský Institute of Physical Chemistry, Czech Academy of Sciences, 182 23 Prague, Czech Republic

⁵Central European Institute of Technology (CEITEC), Brno University of Technology, Purkynova 123, 612 00 Brno, Czech Republic

⁶Institute of Materials Chemistry, Vienna University of Technology (TU Wien), Getreidemarkt 9/165, A-1060 Vienna, Austria

⁷Institute for Applied Physics, University of Tübingen, Auf der Morgenstelle 10, 72076 Tübingen, Germany

^{a)} Authors to whom correspondence should be addressed: stefan.hummel@univie.ac.at; bernhard.bayer-skoff@tuwien.ac.at; and bernhard.bayer@univie.ac.at

ABSTRACT

Suspended membranes of two-dimensional (2D) materials are of interest for many applications. Much of their characterization relies on scanning probe microscopy (SPM) techniques such as atomic force microscopy (AFM) or scanning tunneling microscopy (STM). Unlike rigid samples, the suspended atomically thin 2D membranes are, however, flexible and do not remain mechanically undisturbed during SPM measurements. Local deformations can occur at the location of the scanning tip and thus result in measurements that misrepresent actual membrane topography and nanomechanical properties. Exact levels of such SPM tip-induced deformations in 2D membranes remain largely unknown, as they are to date only indirectly accessible via dual probe microscope concepts that either are not mechanically independent (e.g., SPM-SPM setups resulting in complicated imaging crosstalk) or suffer from intrinsically limited lateral resolution (e.g., optical far-field techniques as the second probe). Circumventing these shortcomings, we here demonstrate that by coupling an AFM with a scanning electron microscope (SEM) as the second, mechanically independent probe, we can directly and *in situ* visualize by SEM at high resolution 2D membrane deformations that result from controllable AFM tip manipulations in the nN range. Employing few-layer graphene as model membranes, we discuss the experimental realization of our coupled *in situ* AFM-SEM approach.

© 2021 Author(s). All article content, except where otherwise noted, is licensed under a Creative Commons Attribution (CC BY) license (<http://creativecommons.org/licenses/by/4.0/>). <https://doi.org/10.1063/5.0040522>

Atomically thin suspended (free-standing) membranes¹ made from two-dimensional (2D) materials are promising for a variety of technological fields including ultra-fast electronics,² nano-electro-mechanical systems (NEMS),³ and highly selective chemical species separation.⁴ A key bottleneck toward realization of many applications is, however, the current lack of available metrology tools to

satisfactorily characterize such mechanically flexible, suspended 2D membranes, in particular in terms of their three-dimensional morphology and their nanomechanical properties. Scanning probe microscopy (SPM) techniques such as atomic force microscopy (AFM) or scanning tunneling microscopy (STM) can potentially access morphology and nanomechanics.^{5–10} We and others have, however,

shown that, unlike for rigid materials/surfaces, SPM techniques do not leave the flexible 2D membranes mechanically undisturbed during measurements.^{11–22} Instead, SPM can result in membrane deformations at the location of the scanning tip. Notably, simulations have suggested that such SPM tip-induced deformations can be larger than the intrinsic topographic features, corrugations or ripples in suspended 2D membranes that one actually aims to measure by SPM.¹⁵ This could result in the worst case in SPM images that completely misrepresent the actual topography and nanomechanics of the membrane, making SPM-based characterization of structural details in suspended 2D membranes challenging and prone to misinterpretation. Conversely, controlled local straining of 2D membranes by SPM-type devices could enable advanced opto-electronic device concepts^{23–27} based on the strain-dependence of opto-electronic properties of many 2D materials.^{13,28–39} For this, however, the exact level of local membrane deformation has also to be known.

While it is now established that SPM is an intrusive microscopy technique for suspended 2D membranes, the exact levels of SPM tip-induced deformations to the 2D membranes remain largely unknown. This is because direct experimental observations of 2D membrane deformations from local SPM-type manipulations are critically lacking. Dual-probe approaches combining SPM with another characterization technique could, in principle, be used to elucidate such local deformations of suspended 2D materials (and of suspended nanomaterials in general) from localized mechanical manipulation. Examples include coupled AFM-STM²¹ and STM-STM,¹⁵ as we have previously demonstrated. In this approach, AFM (or STM) tips contact suspended 2D membranes from opposite sides, upon which the first AFM (or STM) tip deforms the membrane and the opposite second tip measures the deformation induced from the first tip.^{15,21} This approach, however, suffers from the lack of a mechanically independent second probe, as the second AFM (or STM) tip results also in additional membrane deformation and thus only indirect (crosstalk) information on deformation can be extracted.^{15,21} In principle, an independent second probe could be achieved optically, where, in particular, Raman spectroscopy has emerged as a contender to probe 2D materials mechanics due to the high Raman sensitivity to strain.^{19,40} In this, the 2D membrane is deformed by the AFM tip and laterally resolved Raman mapping at and around the location of the scanning AFM tip is concurrently performed, as we have also demonstrated.¹⁹ The Raman signals can then be recalculated to strain profiles in the 2D membrane. This can, however, only result in, at best, indirect inference of morphological sample deformation. Additionally, all optical far-field approaches^{19,40} including also interferometry⁴¹ are inherently limited to a lateral resolution in the region of the wavelength of the employed light, thus setting a lateral resolution limit to ~ 400 nm for visualization of membrane deformations by optical means. This is, however, insufficient to discern intrinsic corrugations or tip-induced deformations of 2D membranes.¹⁵

Here, we demonstrate a dual-probe concept that circumvents these shortcomings of only indirect accessibility of topography and limited lateral resolution. By coupling an AFM with a scanning electron microscope (SEM) as the second (mechanically independent) probe, we directly and *in situ* visualize 2D membrane deformations by SEM that result from controllable AFM tip manipulations. We present our experimental realization of this coupled *in situ* AFM-SEM approach, present the first results for few-layer graphene 2D model

membranes, which yield insights into the nanomechanics of 2D membranes, and discuss the technical challenges encountered.

The implementation of our coupled *in situ* AFM-SEM system [Fig. 1(a)] builds upon a compact AFM system^{42–44} (AFSEMTM, GETec Microscopy GmbH, Austria) that relies on piezo-resistive readout of AFM cantilever deformations, foregoing the need for typically used larger optical cantilever readout systems. This readily allows integration of this AFM module into standard SEM systems (here FEI Quanta 600F, USA). Typically, this combined AFM-SEM is then used in a correlated fashion, i.e., first a fast, larger field of view SEM characterization of a sample is performed, followed by subsequent AFM measurements at the same location.^{42–44} In this correlated use, the self-sensing AFM cantilever is placed directly in the SEM beam path under the SEM's objective lens, thus shielding direct “visual” SEM access to the apex of the sample-probing AFM tip underneath the cantilever. Consequently, this geometry does not allow real *in situ* capabilities toward visualizing AFM tip-induced modification to the sample. We, therefore, instead employ here a geometry in which we tilt the AFM cantilever/tip under the SEM beam in such a way that the AFM tip apex can be seen from the side (under an angle) via the SEM. We thereby obtain direct “visual” access via the SEM to the apex of the AFM tip while the tip is engaged on the sample.^{42,43} To this end, the AFM is mounted on a coarse positioning stage, which is attached to the inner side of the door of the SEM. The AFM is tip-scanner based with the tip as the lowest point of the AFM unit.⁴² Due to the purely electrical readout of the piezo-resistive cantilever, it can easily be moved under the SEM objective lens. While the z-movement and tilt of the SEM stage are coupled to the AFM scanner, i.e., the relative distance of the cantilever and the sample is only determined by the AFM operation (approach, lift-height, etc.), the x-y positioning of the SEM stage is completely decoupled from the AFM part. The tip-scanner and the decoupled x-y SEM positioning, therefore, allows for investigating any spot on the sample also in this tilted geometry. With a typical AFM tip height between 5 and 10 μm , a tilt angle of 35–50° is found to be sufficient for gaining “visual” access to the spot of tip/sample interaction via SEM, as shown below.

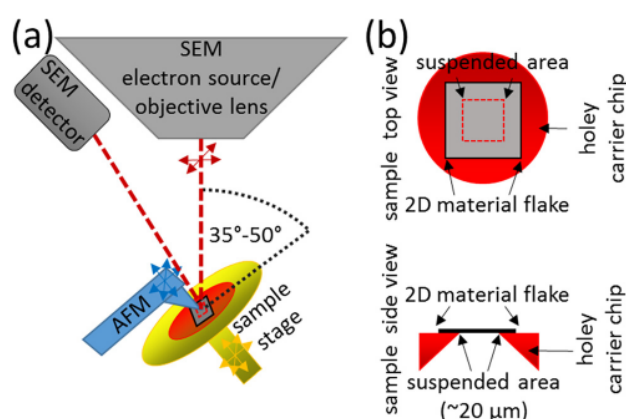


FIG. 1. (a) Schematic illustration of the setup geometry of our coupled *in situ* AFM-SEM system. The arrows indicate free degrees of movement. (b) Schematic illustration of the sample geometry. For a SEM image of a few-layer graphene membrane, see the [supplementary material](#), Fig. S1.

As a model 2D membrane, we use mechanically exfoliated few-layer graphene flakes (~ 5 layers) transferred onto holey silicon carrier chips with single central holes (custom made from Silson Ltd., UK) [Fig. 1(b) and [supplementary material](#), Fig. S1].¹⁹ The transfer employs polymer-grid assistance (Quantifoil, Germany), which partially leaves polymer residues on the membranes ([supplementary material](#), Fig. S1).^{19,21,45} The layer number of the few-layer graphene membranes is checked by optical contrast and Raman spectroscopy.^{19,21} The silicon chips have a thickness of $200\text{ }\mu\text{m}$, into which a pyramid shaped hole is etched by anisotropic etching from the back side of the chip, resulting in an approximately square shape aperture with a lateral size of $\sim 20\text{ }\mu\text{m}$ on the chip's top surface over which the 2D membranes are suspended. The front and back sides of the chip are coated with 5 nm of chromium and 20 nm of gold for electrical conductivity, prior to placing the 2D material membrane. This conductive coating of the sample carriers is found to be crucial to avoid interference of the AFM measurements from charging from the SEM electron beam, see also below. The chips are then glued with silver ink onto a standard SEM stub and mounted in the FEI Quanta 600F SEM. Alternatively, holey SiN TEM membranes (Ted Pella, USA) with arrays of circular $\sim 2\text{ }\mu\text{m}$ diameters holes are used as 2D material carriers (with the same membrane preparation as above). The SEM is evacuated to a base pressure of $\sim 10^{-6}$ mbar. SEM imaging is done using an electron acceleration voltage of 2 keV and an Everhart-Thornley-type secondary electron detector for image acquisition. The AFM tip is brought to the region of interest on the sample using the in-chamber video camera of the SEM for coarse positioning and then using SEM imaging for fine positioning before the AFM tip approach to the sample. As AFM modes, we investigate lateral tip movements under typical contact mode and tapping mode AFM conditions (with feedback on) and nanoindentation force-distance (F-d) curves at selected sample spots. As AFM probes, we employ $100\text{ }\mu\text{m} \times 48\text{ }\mu\text{m}$ cantilevers with single crystal diamond tips attached (SCL-Sensor.Tech. Fabrication GmbH, Austria).

The cantilevers have a resonance frequency of $\sim 268\text{ kHz}$ and a spring constant of $\sim 20\text{ N/m}$. The main reason for choosing diamond tips is a larger tip height of $5\text{--}10\text{ }\mu\text{m}$, which, after tilting under the SEM (to $\sim 40^\circ$), allows for better “visual” access to the AFM tip apex/sample. Cantilever deflection was recalculated to force on the sample for F-d curves using reference measurements on solid Si samples.⁴⁶

Figure 2 shows as a first set of measurements single-point F-d nanoindentation on a region of the few-layer graphene membrane that, prior to the AFM tip approach, appears visually flat in SEM [Fig. 2(a), before contact]. When approaching with the AFM tip, we monitor the force on the membrane from the cantilever [indicated in Fig. 2(a)] and simultaneously acquire SEM images of the tip apex and membrane. A corresponding F-d curve is plotted in Fig. 2(b). We find that the flat region of the membrane deforms under the AFM tip with increasing load. This deformation is hard to resolve by the naked eye in the separated images in Fig. 2(a) but is better apparent in the time-lapsed image sequence in the [supplementary material](#), video V1. Also by calculating the image difference between the $\sim 0\text{ nN}$ (before contact) image and the full load at 2080 nN , we can estimate in the false color plot in Fig. 2(c) that the stretched region in the flat membrane has a lateral extension of $\sim 6\text{ }\mu\text{m}$ for 2080 nN load and 170 nm indentation depth. We note that this reasonably compares with previously measured (by coupled AFM-Raman mapping) lateral strain field extensions of $\sim 7\text{ }\mu\text{m}$ for $\sim 6000\text{ nN}$ load for F-d curves with a similar tip and few-layer graphene membrane.¹⁹ Upon retraction of the AFM tip, the few-layer graphene membrane shows no persistent deformation and again appears similarly flat as before the F-d curve, suggesting that this measurement resulted in solely elastic behavior. Notably, the lateral extent of elastic membrane deformation would not have been directly accessible by sole AFM measurements, but its measurement is facilitated by the coupled *in situ* use of SEM.

Figure 3 extends our investigation from single-point F-d nanoindentation to contact mode AFM movements. In particular, Fig. 3(a)

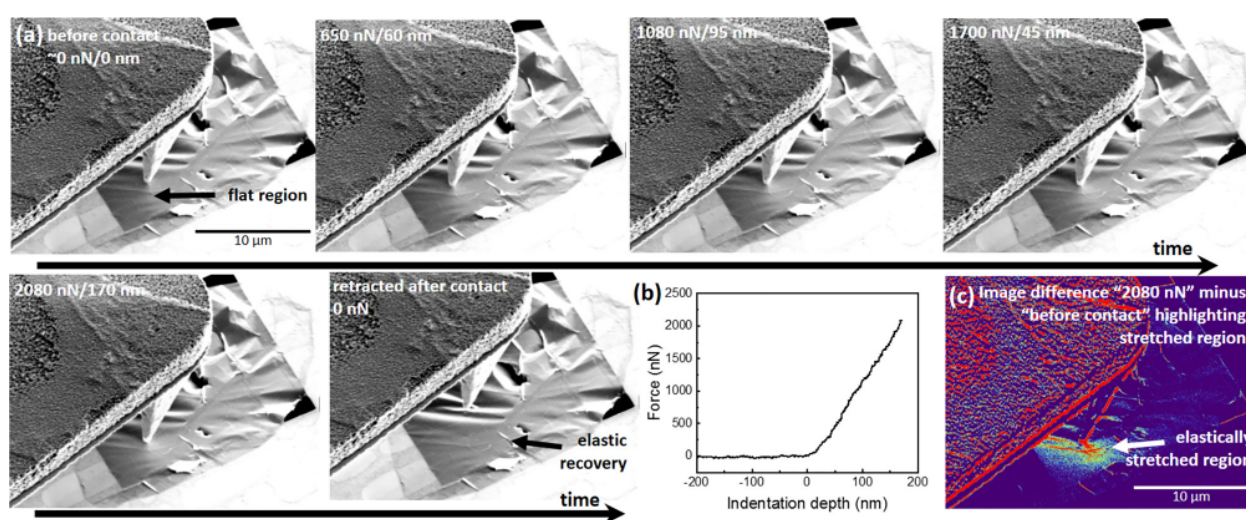


FIG. 2. (a) SEM image sequence during AFM F-d nanoindentation on a flat few-layer graphene membrane region. Corresponding video in the [supplementary material](#), video V1. (b) F-d curve corresponding to nanoindentation as in (a). (c) False-color coded image difference calculated between 2080 nN and before contact images in (a) to emphasize the lateral extent of the elastically stretched membrane region during the nanoindentation.

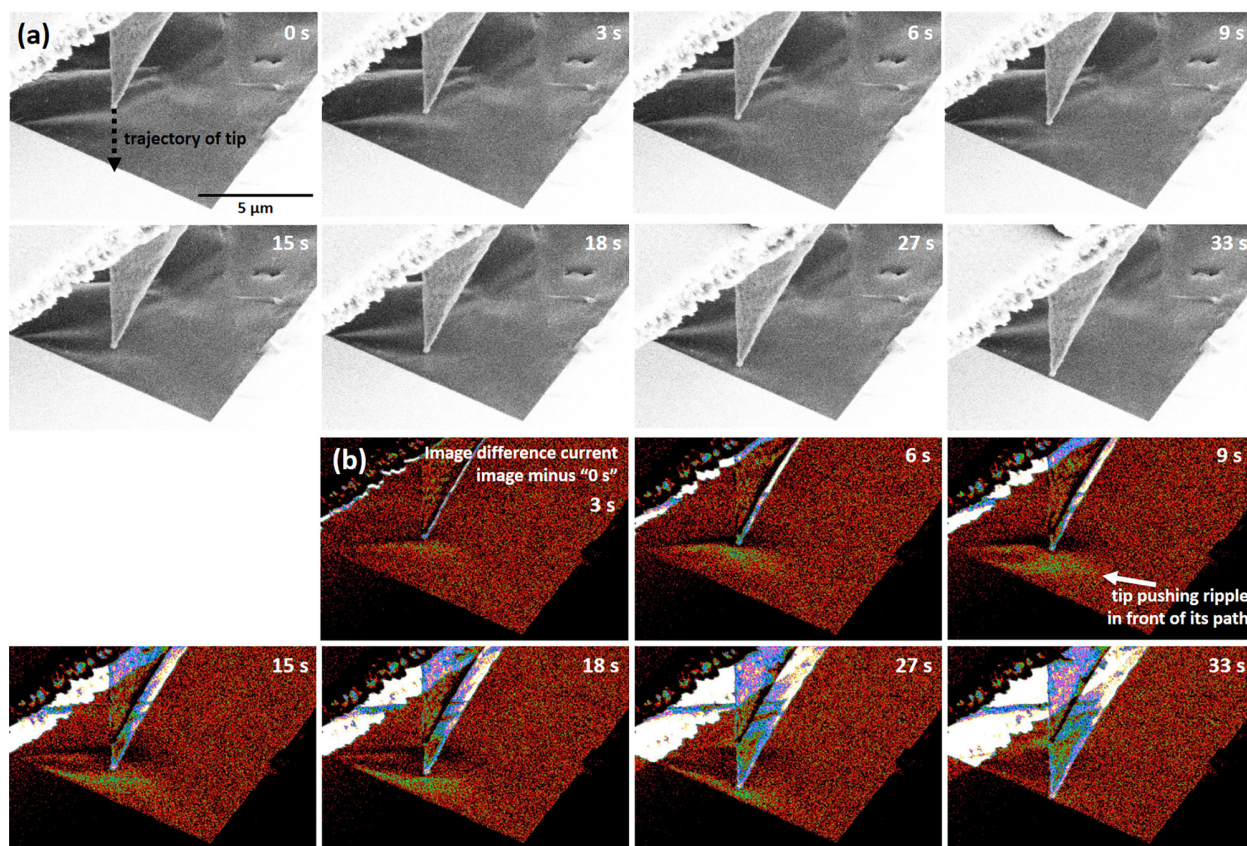


FIG. 3. (a) Time-resolved SEM image sequence during performing an AFM contact mode trajectory (indicated by the arrow) on a flat region of a few-layer graphene membrane. Video in the [supplementary material](#), video V2. (b) False-color coded time-resolved image difference calculated between any current image and the 0 s image in (a) to emphasize the ripple that forms in the membrane preceding the AFM tip's trajectory. Video in the [supplementary material](#), video V3.

shows the effect of an AFM contact mode line movement on the same flat region as in Fig. 2. To acquire this, the AFM tip was first approached to the membrane with a set point of 500 nN, which is a typical setting for contact mode AFM.¹⁹ Then, we move the AFM tip along the indicated trajectory (with feedback on) while simultaneously acquiring the shown SEM video sequence ([supplementary material](#), video V2). To enhance the image details, Fig. 3(b) plots the image difference of the current image in the series with respect to the 0 s image ([supplementary material](#), video V3). We find that as the AFM tip pursues its trajectory, a ripple in the 2D membrane forms in front of the AFM tip and is preceding the tip's path. The ripple is roughly perpendicular to the tip trajectory direction with a lateral width of $\sim 4.5 \mu\text{m}$. This membrane deformation is suggested to be a result of the lateral tip movement and purely elastic in nature, since once the AFM tip leaves the 2D membrane onto the rigid Si support, the morphology of the membrane recovers its initial state. Figure 3 is thereby a direct visualization how an AFM tip deforms a 2D membrane during a contact mode line trajectory. Notably again, using solely an AFM without the coupled *in situ* SEM, it would have not been possible to directly observe this dynamic AFM-tip-induced membrane deformation. In addition to the above-mentioned contact mode experiments, we also

performed AFM tapping mode line trajectories on the few-layer graphene membrane with different typical tapping-mode set-points (95%-60% free space amplitude) while acquiring simultaneous SEM data ([supplementary material](#), video V4). The SEM images recorded during these tapping-mode trajectories did, however, not indicate any AFM-induced deformation of the few-layer graphene membrane. This suggests that typical tapping mode AFM measurements can leave few-layer graphene membranes undisturbed.

In Fig. 4, we perform coupled *in situ* AFM-SEM F-d nanoindentations on a wrinkle in the few-layer graphene membrane [Fig. 4(a) and [supplementary material](#), Fig. S2], which is a typical feature from 2D membrane fabrication.^{15,19,45} In Fig. 4(b), we first observe a stage-wise deformation of the wrinkle under increasing load ([supplementary material](#), video V5). Figure 4(c) shows the corresponding F-d curve. Notably, we find first a monotonically increasing deformation of the wrinkle under the increasing load/indentation depth, until at $\sim 480 \text{ nm}$ indentation depth we observe the wrinkle to suddenly give in, as visualized in the SEM sequence [Fig. 4(b) and [supplementary material](#), video V5) and also indicated via the corresponding force drop in the F-d curve [Fig. 4(c)]. The deformation caused by this F-d nanoindentation is found to be fully reversible [Fig. 4(b), last image],

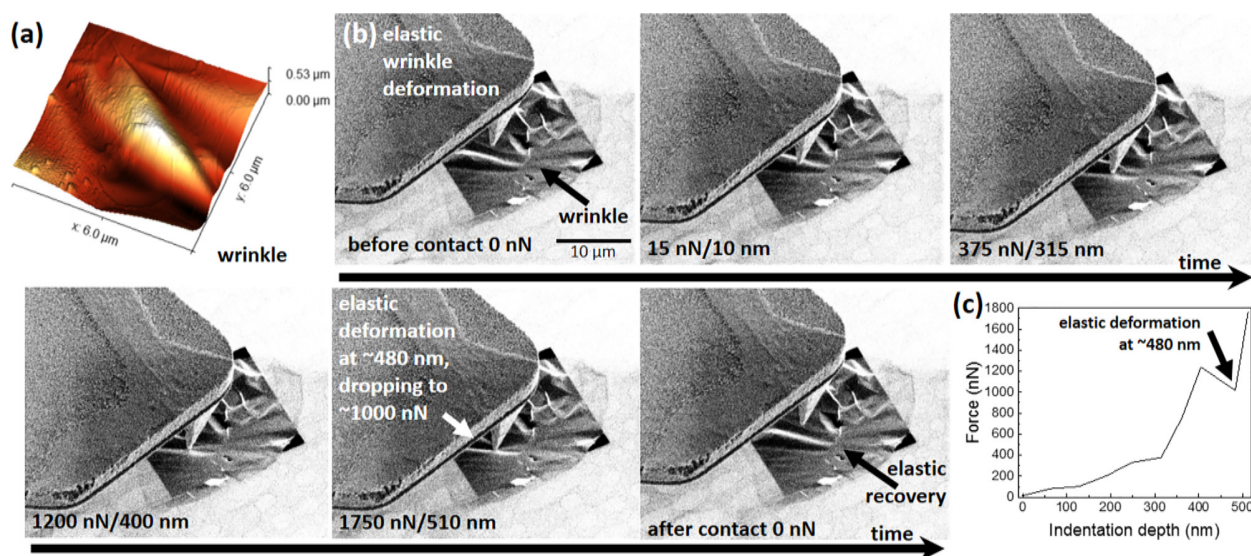


FIG. 4. (a) Three-dimensionally plotted tapping mode AFM image of a fabrication-related wrinkle in the few-layer graphene membrane. Corresponding two-dimensional plot of AFM data in the [supplementary material](#), Fig. S2. (b) SEM image sequence during AFM F-d nanoindentation on the wrinkle from (a), which results in elastic wrinkle deformation. Video in the [supplementary material](#), video V5. (c) F-d curve corresponding to nanoindentation as in (b).

suggesting that this wrinkle deformation was elastic in nature. This is in contrast to the deformation sequence in the [supplementary material](#), Fig. S3 ([supplementary material](#), video V6), which was acquired on the same wrinkle subsequent to Fig. 4(b), but on a slightly different location. After the approach in contact mode, already under a low load of ~ 100 nN we observe in SEM a clear deformation of the wrinkle at the point of contact where a dent forms under the AFM tip apex. With increasing load, this dent deepens and widens and also changes shape. Upon retracting the AFM tip, it becomes apparent that this deformation of the wrinkle is not recovered but persists, suggesting plastic deformation to the membrane by this indentation. The part of the membrane to the right of the AFM tip apex contact actually changed from a convex to a concave surface morphology through the nanoindentation. We note that these direct observations of the intermediate stages of both elastic [Fig. 4(b)] and plastic [[supplementary material](#), Fig. S3] deformation to a 2D membrane are facilitated by the here introduced coupled *in situ* AFM-SEM setup.

Our results demonstrate the capability of coupled *in situ* AFM-SEM to directly visualize at high resolution the local deformations in 2D membranes from local AFM-tip-induced loads with nN control. We have realized our implementation based on a commercial AFM module (AFSEMTM, GETec Microscopy GmbH, Austria) using piezo-resistive self-sensing cantilevers, but note that, in principle, similar measurements should also be possible using conventional optical cantilever readout.^{47,48} During our implementation, we encountered the following experimental challenges: first, the *in situ* AFM-SEM approach requires visual access to the tip apex/sample contact point, which in turn requires the capability to tilt the AFM setup/cantilever/tip and sample with respect to the SEM electron beam. As this is not necessary for typical plan view sequential correlated AFM-SEM, this has to be considered during the implementation design of the AFM module in a particular SEM. An alternative approach could also rely

on the use of “visual access” cantilevers, which allow partial access to the tip apex/sample contact point in plan view and which we have previously used for coupled *in situ* AFM-Raman studies.¹⁹ Second, we found that charging of the AFM cantilever/tip and sample from the SEM’s electron beam has to be minimized, as otherwise electrostatic coupling between the charged cantilever/tip and the sample impedes meaningful AFM positioning. In the worst case scenario, such electrostatic coupling results in unintentional puncture of the 2D membranes upon even gentle AFM tip approaches ([supplementary material](#), Fig. S4). In particular, the charge removal from the sample membrane turned out to be key, which is why the application of a conductive Cr/Au layer on the Si sample carrier prior to 2D flake placement was found to be crucial. Third, the synchronization of AFM scan speeds and SEM image acquisition times has to be maintained. Due to the low SEM signal-to-noise ratio in our particular SEM for the 2D membranes, we here employed rather slow SEM scanning. This resulted in the need to either reduce typical scan speeds in AFM in order to obtain non-blurred images or to even use manual stepwise AFM tip movement (with feedback on) with pauses during SEM images acquisition. For tapping mode AFM in which the tip is oscillating in the kHz region (i.e., much faster than SEM image acquisition time), the tip appears as an overlay of its small amplitude envelope ([supplementary material](#), Video V3 and [supplementary material](#), Fig. S5). Fourth, we here use few-layer graphene membranes (and not monolayers) as testbed model membranes for two reasons: on the one hand, it remains difficult to fabricate monolayer graphene samples suspended over ~ 20 μm holes that can sustain SPM measurements without rupture.¹⁵ Instead, suspended monolayer graphene membranes are often limited to ~ 2 μm diameter holes, which is, however, a much smaller region of interest for dynamic deformations. On the other hand, the here employed SEM had a limited sensitivity to monolayers ([supplementary material](#), Fig. S5). We note that this is, however, not an

intrinsic limitation to the here demonstrated coupled *in situ* AFM-SEM concept, but a limitation stemming from our employed SEM. For, e.g., state-of-the-art field emission gun SEMs or more sensitive SE detectors better detection of graphene monolayers would be possible.^{22,49}

As discussed above, the here presented coupled *in situ* AFM-SEM approach competes with dual SPM probe techniques (STM-STM and AFM-STM),^{15,21} which suffer from mechanically non-independent second probes, and with optical second probes,^{19,40,41} which are limited by the lateral resolution limits of the employed light and, in the case of spectroscopy, are often rather indirect toward morphology elucidation. Additionally, we want to highlight that similar measurements of 2D membrane deformations have recently been shown using micromanipulators in an SEM.²² The difference to using micromanipulators is, however, that with an AFM, the load on the 2D membrane can be more readily controlled with nN accuracy, as we show here.

In summary, we demonstrated the capabilities of coupled *in situ* AFM-SEM to directly visualize by SEM local AFM-tip-induced deformations in suspended 2D membranes using few-layer graphene as a model system. We showed how far elastic deformations during typical F-d nanoindentation laterally extend on a flat 2D membrane region and followed the sequence of elastic and plastic deformations of commonplace non-flat membrane features such as wrinkles. We also directly evidenced that in contact mode AFM movement a ripple in an otherwise flat 2D membrane region can be formed and be pushed in front of the AFM tip by its movement. These observations are related to the nanomechanics of 2D membranes only and they are not limited to our here introduced coupled *in situ* AFM-SEM implementation (albeit these observations are enabled by our implementation). Key considerations to our implementation along with the limitations of this coupled *in situ* AFM-SEM were discussed, to form a basis for further investigations of 2D membrane nanomechanics by coupled *in situ* AFM-SEM.

See the [supplementary material](#) (pdf) for additional *in situ* AFM-SEM, SEM, and AFM data and analyses and captions to [supplementary material](#) videos V1–V6. Supplementary Videos (avi) V1, V2, V3, V4, V5, and V6.

B.C.B., D.Z., and C.S. acknowledge support from the Austrian Research Promotion Agency (FFG) under Project No. 860382-VISION. B.C.B. and O.F. acknowledge support from the Czech-Austrian Scientific Technological Cooperation Program under Grants 8J18AT005/Ministry of Education, Youth and Sports of the Czech Republic and CZ/01–2018/Austrian Agency for International Cooperation (OeAD)/Austrian Federal Ministry of Education, Science and Research. The authors acknowledge the TU Wien Bibliothek for financial support through its Open Access Funding Program.

At the time of performing of this study, S.H. and C.S. have been affiliated with GETec Microscopy GmbH, Austria.

DATA AVAILABILITY

The data that support the findings of this study are available within the article and its [supplementary material](#).

REFERENCES

- ¹X. Zhang and A. Beyer, *Nanoscale* **13**, 1443 (2021).

- ²K. I. Bolotin, K. J. Sikes, Z. Jiang, M. Klima, G. Fudenberg, J. Hone, P. Kim, and H. L. Stormer, *Solid State Commun.* **146**, 351 (2008).
- ³M. C. Lemme, S. Wagner, K. Lee, X. Fan, G. J. Verbiest, S. Wittmann, S. Lukas, R. J. Dolleman, F. Niklaus, H. S. J. van der Zant, G. S. Duesberg, and P. G. Steeneken, *Research* **2020**, 1.
- ⁴L. Wang, M. S. Boutilier, P. R. Kidambi, D. Jang, N. G. Hadjiconstantinou, and R. Karnik, *Nat. Nanotechnol.* **12**, 509 (2017).
- ⁵C. Lee, X. Wei, J. W. Kysar, and J. Hone, *Science* **321**, 385 (2008).
- ⁶D. Garcia-Sanchez, A. M. van der Zande, A. S. Paulo, B. Lassagne, P. L. McEuen, and A. Bachtold, *Nano Lett.* **8**, 1399 (2008).
- ⁷R. Zan, C. Muryn, U. Bangert, P. Mattocks, P. Wincott, D. Vaughan, X. Li, L. Colombo, R. S. Ruoff, B. Hamilton, and K. S. Novoselov, *Nanoscale* **4**, 3065 (2012).
- ⁸L. Tapasztó, T. Dumitrica, S. J. Kim, P. Nemes-Incze, C. Hwang, and L. P. Biro, *Nat. Phys.* **8**, 739 (2012).
- ⁹C. Musumeci, *Crystals* **7**, 216 (2017).
- ¹⁰B. Vasić, M. Kratzer, A. Matković, A. Nevesad, U. Ralević, D. Jovanović, C. Ganser, C. Teichert, and R. Gajić, *Nanotechnology* **24**, 015303 (2013).
- ¹¹T. Mashoff, M. Pratzner, V. Geringer, T. J. Echtermeyer, M. C. Lemme, M. Liebmann, and M. Morgenstern, *Nano Lett.* **10**, 461 (2010).
- ¹²M. Huang, T. A. Pascal, H. Kim, W. A. Goddard, and J. R. Greer, *Nano Lett.* **11**, 1241 (2011).
- ¹³N. N. Klimov, S. Jung, S. Zhu, T. Li, C. A. Wright, S. D. Solares, D. B. Newell, N. B. Zhitenov, and J. A. Strosio, *Science* **336**, 1557 (2012).
- ¹⁴P. Xu, Y. Yang, S. D. Barber, M. L. Ackerman, J. K. Scholz, D. Qi, I. A. Kornev, L. Dong, L. Bellaiche, S. Barraza-Lopez, and P. M. Thibado, *Phys. Rev. B* **85**, 121406 (2012).
- ¹⁵F. R. Eder, J. Kotakoski, K. Holzweber, C. Mangler, V. Skakalova, and J. C. Meyer, *Nano Lett.* **13**, 1934 (2013).
- ¹⁶P. Xu, M. Neek-Amal, S. D. Barber, J. K. Scholz, M. L. Ackerman, P. M. Thibado, A. Sadeghi, and F. M. Peeters, *Nat. Commun.* **5**, 3720 (2014).
- ¹⁷R. Breitwieser, Y.-C. Hu, Y. C. Chao, R.-J. Li, Y. R. Tzeng, L.-J. Li, S.-C. Liou, K. C. Lin, C. W. Chen, and W. W. Pai, *Carbon* **77**, 236 (2014).
- ¹⁸M. Neek-Amal, P. Xu, J. K. Scholz, M. L. Ackerman, S. D. Barber, P. M. Thibado, A. Sadeghi, and F. M. Peeters, *Nat. Commun.* **5**, 4962 (2014).
- ¹⁹K. Elibol, B. C. Bayer, S. Hummel, J. Kotakoski, G. Argentero, and J. C. Meyer, *Sci. Rep.* **6**, 28485 (2016).
- ²⁰W. Ko, S. M. Hus, X. Li, T. Berlijn, G. D. Nguyen, K. Xiao, and A.-P. Li, *Phys. Rev. B* **97**, 125401 (2018).
- ²¹K. Elibol, S. Hummel, B. C. Bayer, and J. C. Meyer, *Sci. Rep.* **10**, 4839 (2020).
- ²²P. Schweizer, C. Dolle, D. Dasler, G. Abellán, F. Hauke, A. Hirsch, and E. Spiecker, *Nat. Commun.* **11**, 1743 (2020).
- ²³J. Feng, X. Qian, C.-W. Huang, and J. Li, *Nat. Photonics* **6**, 866 (2012).
- ²⁴H. Zhu, Y. Wang, J. Xiao, M. Liu, S. Xiong, Z. J. Wong, Z. Ye, Y. Ye, X. Yin, and X. Zhang, *Nat. Nanotechnol.* **10**, 151 (2015).
- ²⁵M. M. Benameur, F. Gargiulo, S. Manzeli, G. Autes, M. Tosun, O. V. Yazyev, and A. Kis, *Nat. Commun.* **6**, 8582 (2015).
- ²⁶S. Manzeli, A. Allain, A. Ghadimi, and A. Kis, *Nano Lett.* **15**, 5330 (2015).
- ²⁷S. Song, D. H. Keum, S. Cho, D. Perello, Y. Kim, and Y. H. Lee, *Nano Lett.* **16**, 188 (2016).
- ²⁸M. Mohr, K. Papagelis, J. Maultzsch, and C. Thomsen, *Phys. Rev. B* **80**, 205410 (2009).
- ²⁹G.-X. Ni, H.-Z. Yang, W. Ji, S.-J. Baeck, C.-T. Toh, J.-H. Ahn, V. M. Pereira, and B. Özyilmaz, *Adv. Mater.* **26**, 1081 (2014).
- ³⁰E. Scalise, M. Houssa, G. Pourtois, V. Afanas'ev, and A. Stesmans, *Nano Res.* **5**, 43 (2012).
- ³¹K. He, C. Poole, K. F. Mak, and J. Shan, *Nano Lett.* **13**, 2931 (2013).
- ³²C. Rice, R. J. Young, R. Zan, U. Bangert, D. Wolverson, T. Georgiou, R. Jalil, and K. S. Novoselov, *Phys. Rev. B* **87**, 081307 (2013).
- ³³A. Castellanos-Gomez, R. Roldán, E. Cappelluti, M. Buscema, F. Guinea, H. S. J. van der Zant, and G. A. Steele, *Nano Lett.* **13**, 5361 (2013).
- ³⁴G. W. Jones and V. M. Pereira, *New J. Phys.* **16**, 093044 (2014).
- ³⁵H. Li, A. W. Contryman, X. Qian, S. M. Ardakani, Y. Gong, X. Wang, J. M. Weisse, C. H. Lee, J. Zhao, P. M. Ajayan, J. Li, H. C. Manoharan, and X. Zheng, *Nat. Commun.* **6**, 7381 (2015).
- ³⁶U. Ludacka, M. Monazam, C. Rentenberger, M. Friedrich, U. Stefanelli, J. Meyer, and J. Kotakoski, *npj 2D Mater. Appl.* **2**, 1 (2018).

- ³⁷Z. Peng, X. Chen, Y. Fan, D. J. Srolovitz, and D. Lei, *Light Sci. Appl.* **9**, 1 (2020).
- ³⁸R. Höller, V. Smejkal, F. Libisch, and C. Hellmich, *Int. J. Eng. Sci.* **154**, 103342 (2020).
- ³⁹R. Höller, F. Libisch, and C. Hellmich, *Mech. Adv. Mater. Struct.* (published online, 2020).
- ⁴⁰J. Zabel, R. R. Nair, A. Ott, T. Georgiou, A. K. Geim, K. S. Novoselov, and C. Casiraghi, *Nano Lett.* **12**, 617 (2012).
- ⁴¹D. Davidovikj, J. J. Slim, S. J. Cartamil-Bueno, H. S. van der Zant, P. G. Steeneken, and W. J. Venstra, *Nano Lett.* **16**, 2768 (2016).
- ⁴²J. Kreith, T. Strunz, E. Fantner, G. Fantner, and M. Cordill, *Rev. Sci. Instrum.* **88**, 053704 (2017).
- ⁴³J. Sattelkow, J. E. Fröch, R. Winkler, S. Hummel, C. Schwalb, and H. Plank, *ACS Appl. Mater. Interfaces* **11**, 22655 (2019).
- ⁴⁴S. H. Andany, G. Hlawacek, S. Hummel, C. Brillard, M. Kangül, and G. E. Fantner, preprint [arXiv:200400536](https://arxiv.org/abs/200400536) (2020).
- ⁴⁵M. Kratzer, B. C. Bayer, P. R. Kidambi, A. Matković, R. Gajić, A. Cabrero-Vilatela, R. S. Weatherup, S. Hofmann, and C. Teichert, *Appl. Phys. Lett.* **106**, 103101 (2015).
- ⁴⁶See www.jpk.com/jpk-tech-force-spectroscopy-14-2.download.c46f64176d66c310620d0c4bdf4be7ef for “A practical guide to AFM force spectroscopy and data analysis,” JPK Technical Note.
- ⁴⁷N. Anspach, F. Hitzel, F. Zhou, and S. Eyhusen, *Microsc. Microanal.* **20**, 992 (2014).
- ⁴⁸See www.youtube.com/watch?v=upaX7t_rh3E for implementation of AFM-SEM via optical cantilever deflection read-out.
- ⁴⁹A. Niggas, J. Schwestka, S. Creutzburg, T. Gupta, D. Eder, B. Bayer, F. Aumayr, and R. Wilhelm, *J. Chem. Phys.* **153**, 014702 (2020).